

Article

Effect of Basicity on the Sulfur Precipitation and Occurrence State in Kambara Reactor Desulfurization Slag

Renlin Zhu ¹, Jianli Li ^{1,2,3,*} , Jiajun Jiang ², Yue Yu ² and Hangyu Zhu ² 

- ¹ The State Key Laboratory of Refractories and Metallurgy, Wuhan University of Science and Technology, Wuhan 430081, China; zhurenlin522425@wust.edu.cn
- ² Hubei Provincial Key Laboratory for New Processes of Ironmaking and Steelmaking, Wuhan University of Science and Technology, Wuhan 430081, China; 0204039@wust.edu.cn (J.J.); yuyue@wust.edu.cn (Y.Y.); zhuhy@wust.edu.cn (H.Z.)
- ³ Key Laboratory for Ferrous Metallurgy and Resources Utilization of Ministry of Education, Wuhan University of Science and Technology, Wuhan 430081, China
- * Correspondence: jli@wust.edu.cn

Abstract: Kambara Reactor (KR) desulfurization slag used as slag-making material for converter smelting can promote early slag melting in the initial stage and improve the efficiency of dephosphorization. However, its direct utilization as a slagging material can increase the sulfur content in molten steel since KR desulfurization slag contains 1~2.5% sulfur. Therefore, this research focuses on the effect of basicity on the precipitation behavior and occurrence state of sulfur in KR desulfurization slag in order to provide an academic reference for the subsequent removal of sulfur from slag through an oxidizing atmosphere. The solidification process of slag was simulated by the Factsage8.0. The slag samples were analyzed by X-ray diffraction (XRD) and scanning electron microscope (SEM), and the amount of CaS grains was analyzed using Image-ProPlus6.0 software. The thermodynamic calculation showed that the crystallization temperature of CaS in the molten slag gradually decreased with the increase in basicity, and the CaS crystals in the molten slag mainly existed in the matrix phase and at the silicate grain boundaries. A large number of CaS grains were precipitated along the silicate grain boundary in low-basicity ($R = 2.5$ and 3.0) slags and fewer CaS grains were precipitated along the silicate grain boundary, while the CaS grain density in the matrix phase was higher in the high-basicity ($R = 3.5, 4.0, 4.5$) slag. With the increase in basicity, the number of CaS grains gradually decreased, and the CaS grain sizes in slag sample increased gradually. The sulfur in the synthetic slag was in the form of CaS crystals and the amorphous phase, and the content of amorphous sulfur gradually increased with increasing basicity.

Keywords: KR desulfurization slag; basicity; CaS; precipitation; occurrence



Citation: Zhu, R.; Li, J.; Jiang, J.; Yu, Y.; Zhu, H. Effect of Basicity on the Sulfur Precipitation and Occurrence State in Kambara Reactor Desulfurization Slag. *Minerals* **2021**, *11*, 977. <https://doi.org/10.3390/min11090977>

Academic Editors: Chiharu Tokoro, Shuai Wang, Xingjie Wang and Jia Yang

Received: 12 August 2021

Accepted: 4 September 2021

Published: 8 September 2021

Publisher's Note: MDPI stays neutral with regard to jurisdictional claims in published maps and institutional affiliations.



Copyright: © 2021 by the authors. Licensee MDPI, Basel, Switzerland. This article is an open access article distributed under the terms and conditions of the Creative Commons Attribution (CC BY) license (<https://creativecommons.org/licenses/by/4.0/>).

1. Introduction

Sulfur is a detrimental impurity in molten steel that can easily form long strips or flake-shaped sulfide inclusions, causing a decrease in the transverse compressive strength and plasticity of steel [1]. In addition, the FeS formed in molten steel easily shapes a low-temperature eutectic at the grain boundary of ferrite and austenite, which reduces the hot workability of steel [2]. Lv et al. [3] conducted a study about the effect of sulfur on the properties of high-manganese austenitic steel and discovered that an increase in sulfur content leads to a decrease in the ductility and plasticity temperature range of high-manganese austenitic steel. To reduce the effect of sulfur on the performance of steel, metallurgical enterprises often pretreat blast furnace hot metal for desulfurization outside the furnace. At present, the commonly used domestic hot metal desulfurization pretreatment processes outside the furnace mainly include the KR desulfurization process and the injection desulfurization process [4,5]. The KR desulfurization process involves inserting the poured cross-shaped refractory stirring head into the molten iron to a certain

depth, and then driving it at a certain speed to rotate in the molten iron to produce a vortex. Then, the desulfurizer and the molten iron are fully contacted to achieve a desulfurization effect [6]. In the injection desulfurization process, inert gas and desulfurizer are injected into the molten iron at the same time by a spray gun, and the inert gas plays the main role of carrying the desulfurizer and stirring the molten iron [7,8]. Due to the superior dynamic conditions and high desulfurization efficiency of the KR mechanical stirring desulfurization process, it has gradually replaced the injection desulfurization process and has become the most widely used hot metal pretreatment desulfurization process in China [9]. However, the widespread use of the KR desulfurization process in China is leading to an increase in the output of KR desulfurization slag, causing the accumulation of KR desulfurization slag, occupying a large amount of land resources, and polluting the surrounding waters and atmospheric environment of enterprises. It can be concluded that improving the comprehensive utilization rate of KR desulfurization slag is extremely important for environmentally friendly production within enterprises.

The composition of KR desulfurization slag comprises CaO, SiO₂, MgO, Al₂O₃, CaF₂, CaS and MFe, and the sulfur content is 1.0~2.5% [10]. At present, the treatments of KR desulfurization slag in domestic and foreign enterprises mainly include recovering MFe from the slag and reusing the tailing as sintering ingredients, building materials etc. [11–14]. Han et al. [11] used the combined process of grinding classification–gravity, separation–magnetic and separation to extract iron from desulfurization slag of Angang, and the TFe grade of the iron concentrate reached 86.32%, the S grade decreased to 0.21%, and an iron recovery rate of 78.48% in the slag was achieved. Sheng et al. [12] studied the comprehensive utilization of KR desulfurization slag in neutralizing acid mine wastewater and found that KR desulfurization slag can effectively neutralize acid mine wastewater, although there is little f-CaO in the slag. Fujino et al. [14] reported that the application of KR desulfurization slag in sintering production can reduce coking coal consumption, increase the melt, and reduce CO₂ emission in the sintering process. However, if the use of KR desulfurization slag exceeds 15%, the permeability of the sintering bed will be decreased. In addition, Nakai et al. [15] showed that adding 70% KR desulfurization slag for hot metal pretreatment desulfurization has the same desulfurization capacity as using pure desulfurizer (CaO-5%CaF₂) and can save 40% desulfurizer consumption. In summary, the above research has promoted the technical development of the comprehensive utilization of KR desulfurization slag to varying degrees, but the above process does not consider the removal of sulfur in slag to improve the value of the comprehensive utilization of KR desulfurization slag. Furthermore, the economic benefit of the above processes for the utilization of KR desulfurization slag is low. CaF₂ and CaS in the slag easily produce the toxic gases HF and H₂S due to reacting with the moisture in air, resulting in secondary pollution. Therefore, developing new techniques for the comprehensive utilization of KR desulfurization slag is of great significance to the long-term development of enterprises.

The main component of KR desulfurization slag is CaO, which is mostly contained in the form of silicate (2CaO·SiO₂, 3CaO·SiO₂) and f-CaO in KR slag [16]. If KR desulfurization slag replaces the reactive lime for converter slag making, it can promote early slag melting in the initial stage of converter smelting and can improve the efficiency of converter dephosphorization. Relevant researchers [17–19] have reported that C2S can form a stable solid solution C2S-C3P (2CaO·SiO₂-3CaO·P₂O₅) with C3P (3CaO·P₂O₅) to improve the stability of phosphorus in the molten slag. To this end, the reuse of KR desulfurization slag in converter smelting process has been studied. Jiang et al. [20] concluded that the average sulfur content is 0.0136% higher than in the normal converter smelting process. It can be seen that reusing KR desulfurization slag for converter smelting directly increases the sulfur content and reduces the quality of molten steel. Therefore, in order to compensate for the shortcomings of the current smelting process, the thermodynamic database Factsage8.0 was used herein to simulate the solidification process of slag, as well as XRD and SEM-EDS were used to analyze and detect the mineral phase and microstructure of slag to investigate the effect of basicity on the sulfur precipitation behavior and occurrence state

of KR desulfurization slag in the form of synthetic slag to provide a theoretical basis for the subsequent removal of sulfur in KR desulfurization slag through an oxidizing atmosphere and realize the comprehensive utilization of KR desulfurization slag in the converter smelting process.

2. Experimental Procedure

2.1. Synthetic Slag Composition

According to the existing conclusions and the desulfurization principle of the KR desulfurization process, it can be determined that sulfur in slag mainly exists in the form of a CaS phase [21]. Therefore, the sulfur in synthetic slag was added in the form of CaS, and the mass fraction was 3.38% (1.5% S). CaO, SiO₂, Al₂O₃, MgO and CaF₂ were all analytical pure chemical reagents. According to industrial KR desulfurization slag, the basicity of synthetic slag was set to 2.5, 3.0, 3.5, 4.0, and 4.5. The mass fractions of Al₂O₃ and MgO in the synthetic slag were controlled to be 6.00% and 3.00%, respectively. The CaO and SiO₂ contents in the synthetic slag were added according to binary basicity. The mass ratio of CaF₂ and CaO in the slag was 1:9. The chemical compositions of synthetic slags with different basicities in the CaO-SiO₂-CaF₂-CaS-based system are shown in Table 1.

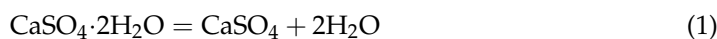
Table 1. Chemical composition of molten slag, wt.%.

Sample	CaO	SiO ₂	Al ₂ O ₃	MgO	CaS	CaF ₂	CaO%/SiO ₂ %
S1	59.23	23.69	6.00	3.00	3.38	6.58	2.50
S2	61.96	20.65	6.00	3.00	3.38	6.88	3.00
S3	64.07	18.31	6.00	3.00	3.38	7.12	3.50
S4	65.76	16.44	6.00	3.00	3.38	7.31	4.00
S5	67.13	14.92	6.00	3.00	3.38	7.46	4.50

2.2. Preparation Process of Synthetic Slag

The laboratory preparation of synthetic slag mainly includes the laboratory preparation of CaS and synthetic slag samples with different basicities in Table 1.

In the beginning, CaS added into synthetic slag was prepared through high-temperature carbothermal reduction in the laboratory because CaS is apt for oxidation. The raw materials for preparing CaS are carbon powder (purity > 99.85%) and CaSO₄·2H₂O (purity > 99.95%). CaSO₄·2H₂O was first heated at 200 °C for 2 h to dehydrate and form CaSO₄, and then the dehydrated CaSO₄ was mixed with carbon powder in a molar ratio of 1:2 and loaded into the corundum crucible. Then, the corundum crucible was placed in the constant temperature zone of the carbon-tube furnace with nitrogen atmosphere at a flow rate of 1L/min. The heating rate was set to 10 °C/min, and the reaction temperature was set to 1100 °C. Finally, after holding at 1100 °C for 2 h, the sample was cooled to room temperature in a nitrogen atmosphere and the CaS purity was calculated. The principle of CaS preparation in the laboratory are shown in Equations (1) and (2).



Second, the quality of the synthetic slag sample was determined to be 100 g, and the analytical pure chemical reagents were precisely weighed according to the different slag compositions shown in Table 1. Furthermore, the chemical reagents were fully stirred and evenly screened twice with 35 mesh and 200 mesh standard screens. The mixed synthetic slag was placed into the corundum crucible, and the corundum crucible was placed in the constant temperature zone of the carbon-tube furnace. The nitrogen flow rate of the carbon-tube furnace was set to 1 L/min, the reaction temperature was set to 1600 °C, and the heating rate was 15 °C/min. The slag sample was extracted by a quartz glass tube when the holding times reached 15 min.

2.3. Analysis Method

In order to clarify the evolution process of mineral composition and slag microstructure with basicity in different slag samples. The samples S1–S5 were detected by X-ray diffraction analyzer (XRD, Rigaku/SmartLab SE, Tokushima, Tokyo, Japan). The detection data of the X-ray diffractometer were analyzed by Search-Match software, and the data were plotted by Origin2019. Moreover, the microstructure of different slag samples was analyzed by SEM-X spectrometry (SEM-EDS; ThermoFisher/Apreo S HiVac, Wyman Street, Waltham, MA, USA). Finally, the amount of CaS grains in different slag samples were analyzed by Image-ProPlus 6.0 (IPP6.0, Media Cybernetics, Bethesda, MD, USA).

3. Thermodynamic Calculation of Synthetic Slag Solidification

The Equilib module of the thermodynamic database FactSage (FactSage 8.0, GTT, Germany) was used to simulate the equilibrium solidification process of the S3 sample with FToxid and FTsalt. In the software, the pure liquids and pure solids of the compound species of the production were chosen. The simulation temperature range was 1100–1600 °C, and the calculation step was set as 10 °C/min. The results are shown in Figure 1. When the temperature was 1600 °C, two phases coexisted in the molten slag, namely, the liquid phase and the MeO#1 phase (CaO solid solution). When the temperature decreased to 1420 °C, the C2S phase began to precipitate from the liquid phase; when the temperature was lower than 1340 °C, the sulfur in the residual liquid began to precipitate in the form of CaS; when the temperature was lower than 1320 °C, the MeO#2 phase (MgO solid solution) and the $12\text{CaO}\cdot 7\text{Al}_2\text{O}_3\cdot \text{CaF}_2$ phase began to precipitate from liquid phase; when the temperature decreased to 1275 °C, the precipitation content of MeO#1 and C2S increased simultaneously. When the temperature decreased to 1150 °C, all phases in the synthetic slag were completely precipitated. It can be seen from Figure 1 that the MeO#2 phase and CaS were mainly precipitated in the form of pure substance during solidification, and no chemical reaction occurred with the other components in the molten slag, while the sulfur in the slag completely precipitated into the CaS phase. Moreover, Al_2O_3 reacted with CaF_2 and CaO in the slag to form the low-melting point compound $12\text{CaO}\cdot 7\text{Al}_2\text{O}_3\cdot \text{CaF}_2$.

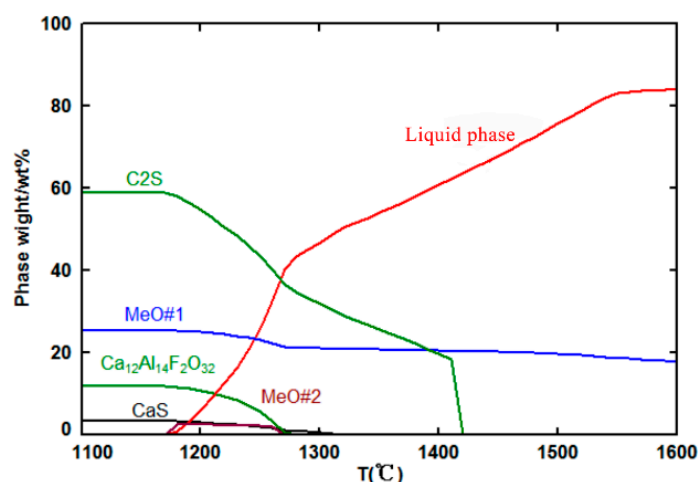


Figure 1. Solidification simulation analysis of synthetic slag S3.

Second, the amount of precipitation of each phase vs. basicity is plotted in Figure 2, indicating that the amount of precipitation amount of the CaS, MeO#2 and $12\text{CaO}\cdot 7\text{Al}_2\text{O}_3\cdot \text{CaF}_2$ phases in the molten slag remained the same quality with an increase in basicity. This is because the contents of MgO and CaS in the different synthetic slags were 3.00 and 3.38 g, respectively, and the sulfur and magnesium in the slag were able to completely precipitate. According to the thermodynamic calculation in Figure 1, MgO and CaS did not react with the other components in the slag during solidification, and they could completely precipitate into MeO#2 phase (MgO solid solution) and CaS during solidification. Additionally,

the complete precipitation of $12\text{CaO}\cdot 7\text{Al}_2\text{O}_3\cdot \text{CaF}_2$ in slag was unaffected by the change in basicity, mainly due to CaO being the main composition in the synthetic slag, in the molten state, Al_2O_3 in slags with different basicities completely reacted with CaO and CaF_2 to form $12\text{CaO}\cdot 7\text{Al}_2\text{O}_3\cdot \text{CaF}_2$. Moreover, when the basicity increased from 2.5 to 4.5, the C2S phase decreased from 72.62% to 48.05%, and the amount of precipitation of MeO#1 phase increased from 10.25% to 34.82% in the solid slag. The amount of precipitation of C2S phase in the slag was negatively correlated with the increase in basicity, while the amount of precipitation of the MeO#1 phase was positively correlated.

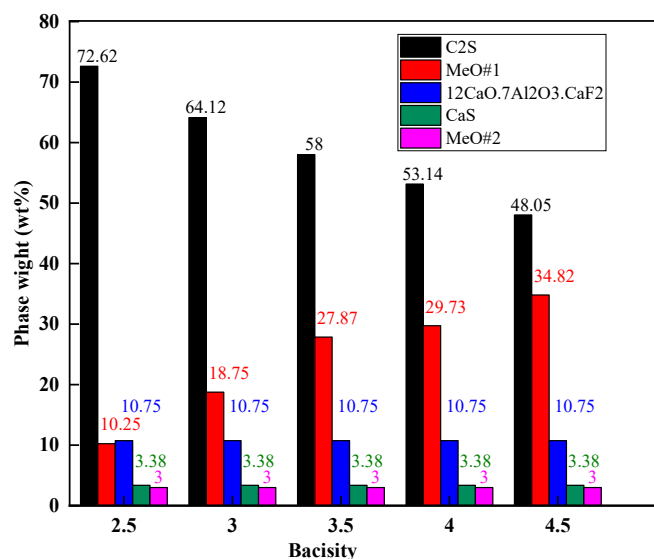


Figure 2. Relationship between the total amount of precipitation of each phase in the solid slag and the basicity.

Since the slag samples were prepared in the laboratory at $1600\text{ }^\circ\text{C}$, the thermodynamic analysis of the molten slag phase at $1600\text{ }^\circ\text{C}$ was calculated to provide a reference for the mineral structure in molten slags with different basicities; the calculation result is shown in Figure 3. It was observed that all slag samples were composed of MeO#1 and liquid phases at $1600\text{ }^\circ\text{C}$. With the increase in basicity from 2.5 to 4.5, the liquid phase content in the molten slag decreased from 96.26% to 73.63%, while the MeO#1 phase content increased from 3.74% to 26.37%. It can be concluded that the supersaturation of MeO#1 phase in molten slag increased with the increase in basicity at $1600\text{ }^\circ\text{C}$.

Moreover, the process of sulfur precipitation in molten slag is related to the crystallization temperature of its sulfur; thus, the thermodynamic calculation of the crystallization temperature of sulfur in slag can provide a theory for the analysis of sulfur precipitation behavior in molten slag. The crystallization temperature of CaS in different basicities slag was calculated as shown in Figure 4. When the basicity was 2.5, the highest crystallization temperature of CaS was $1340\text{ }^\circ\text{C}$. When the basicity was 4.5, the crystallization temperature of CaS was $1305\text{ }^\circ\text{C}$. Thus, it can be seen that the crystallization temperature of CaS was a strong function of basicity. The increase in basicity tended to promote a lower crystallization temperature, and the temperature decreased from $1340\text{ }^\circ\text{C}$ to $1305\text{ }^\circ\text{C}$.

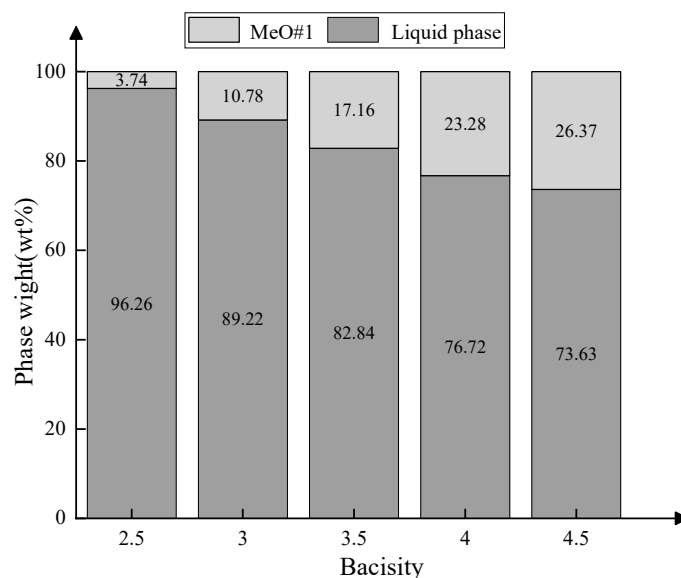


Figure 3. Relationship between the molten slag phase and the basicity at 1600 °C.

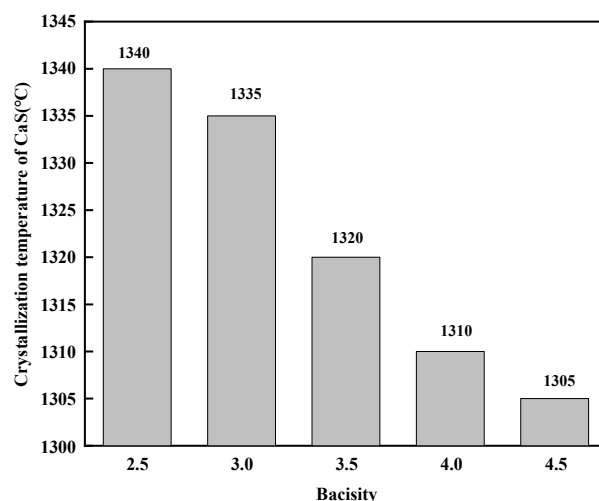


Figure 4. Diagram of the relationship between the crystallization temperature and the basicity of CaS in molten slag.

Based on the above solidification simulation analysis of each phase in the molten slag, the sulfur in the slag was precipitated in the form of CaS minerals, and the basic phases in the molten slag were C_2S , MeO#1, MeO#2, $12CaO \cdot 7Al_2O_3 \cdot CaF_2$ and CaS. Two phases coexisted in the molten slag at 1600 °C, and the particle concentration of the MeO#1 phase increased with the increase of basicity. During the equilibrium solidification process, the sulfur in the slag completely precipitated in the form of a CaS phase, and the crystallization temperature of CaS in the slag gradually decreased with the increase in basicity.

4. Results

4.1. Analysis of Synthetic Slag

Figure 5 presents the XRD analysis results of the synthetic slag samples with different basicities. The corresponding phase was C_3S at diffraction angles of 32.3° , 32.7° , 34.4° , 41.5° , 51.9° and 62.4° . The corresponding phase was C_2S at diffraction angles of 32.3° , 32.7° and 41.5° . The corresponding phase was CaS at diffraction angles of 31.5° , 45.2° and 60.2° , and MeO#2 at diffraction angles of 36.3° , 43.4° and 62.5° . When a slag basicity of $R \leq 3.5$, the characteristic peak of the MeO#1 phase didn't appear in the solid slag. When the basicity increased to 4.0, the characteristic peak of the MeO#1 phase began to appear at

2θ of 32.5° , 37.2° , and 54.5° , and the intensity of the characteristic peak of the MeO#1 phase gradually enhanced with the increase in basicity. This was mainly because the basicity of the slag was less than or equal to 3.5, the CaO in the slag was in an unsaturated state in the actual melting process, and CaO completely reacted with the other components in the slag to form silicate in the heat preservation process. Furthermore, when the basicity was greater than or equal to 4.0, the MeO#1 phase in the slag gradually increased due to the basicity being greater than or equal to 4.0, the supersaturation of the CaO content in the slag gradually increased, which caused the content of the MeO#1 phase that precipitated in the slag during solidification to gradually increase. Based on the above analysis, it can be concluded that the basic mineral phases of the solid slag were the silicate phase (C_2S and C_3S), the MeO#2 phase and the CaS phase, when the basicity was 2.5, 3.0 or 3.5; the basic mineral phases of the solid slag included the silicate phase (C_2S and C_3S), the MeO#1 phase (CaO solid solution), the MeO#2 phase (MgO solid solution) and the CaS phase, when the basicity was 4.0 or 4.5.

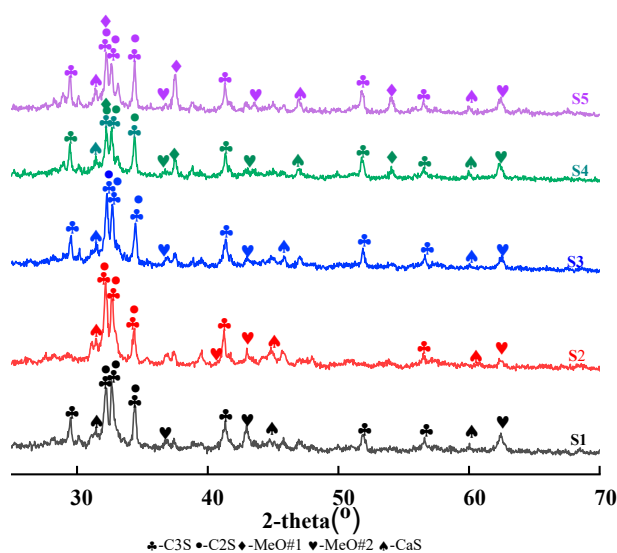


Figure 5. XRD diagram of synthetic slags with different basicities.

In addition, the thermodynamic calculations in Figures 1 and 2 show that the main phase in solid slag was the C_2S phase, but the experimental results conclude that the silicate phase were C_2S and C_3S in solid slag. The main reason for the phenomenon is that the Equilib module of the thermodynamic database Factsage8.0 lacks C_3S data. Therefore, the thermodynamic calculation results showed that the slag contained only C_2S phase.

4.2. Microstructure of the Slag Samples

Figure 6 shows the synthetic slag samples with different basicities prepared at 1600°C and 1 L/min nitrogen for 15 min. According to the results of EDS, C_2S , C_3S , matrix, MeO#1, MeO#2 phase and CaS phases were determined in solid slag samples, a- C_3S , b- C_2S , c-matrix, d-MeO#2, e-CaS and f-MeO#1 phase. When the basicity was 2.5, the solid slag mainly contained long-strip C_3S phase and small particle C_2S -phase, while the CaS and black MeO#2 phase dispersed in the silicate grain boundary and matrix phase. When the basicity was 3.0, the C_2S phase in the molten slag was round structure and the content was more than that in S1, while the content of the C_3S phase was less than that in S1. The MeO#2 phase in slag sample S2 was mainly distributed at the grain boundary of the C_2S phase or C_3S phase. In addition, the CaS grains in S2 were mainly distributed at the grain boundaries of the round cake-like C_2S phase, and the CaS grains were larger than those in S1. When the basicity of the molten slag was 3.5, the C_3S phase was mainly distributed in the slag with a large area of block structures, and a small amount of dispersion was distributed in the matrix phase, while there was no obvious single C_2S phase in the solid

slag. Furthermore, the MeO#2 phase began to grow up in the black block structure, and the larger dimensional CaS grains began to increase. When the basicity of the slag was 4.0 and 4.5, the content of the C3S phase in the slag was more than that of S3, the grain area of the MeO#2 phase was larger than that in S3, while the white CaS phase was distributed at the grain boundary of the C3S phase in strip and particle shapes. Moreover, the porous oval MeO#1 phase began to appear in S4 slag samples, the number of MeO#1 phase grains in S5 was higher than that in the S4. XRD analysis results showed that the slag with different basicity contained C2S phase, but EDS analysis of slag only S1, S2 contained a large number of C2S phase. S3, S4, S5 did not contain C2S phase due to the main silicate product of S3, S4 and S5 slag samples with high basicity being C3S in the heat preservation process.

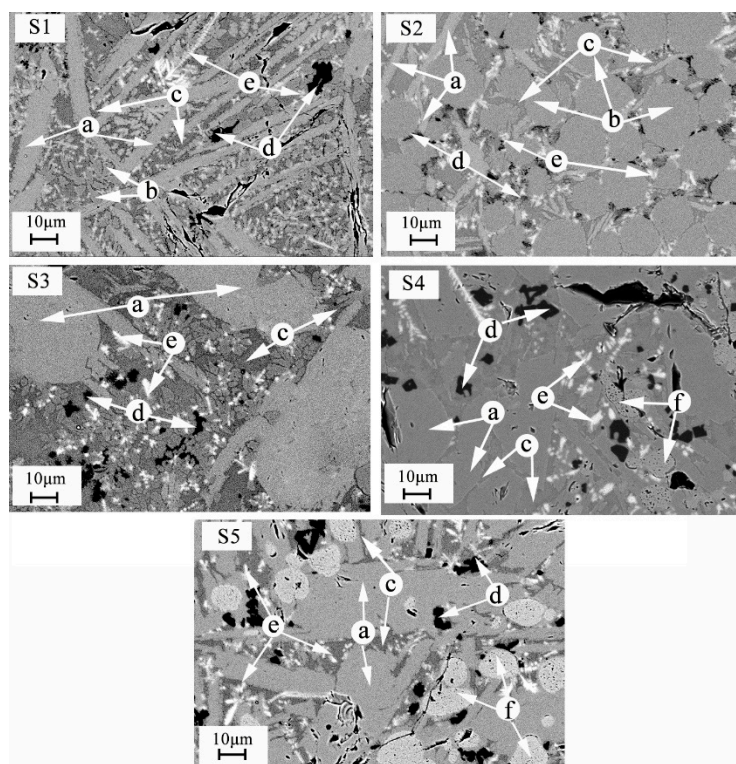


Figure 6. Micro analysis chart of slag samples with different basicity. a, C3S; b, C2S; c, matrix phase; d, MeO#2 phase; e, CaS phase; f, MeO#1 phase. S1—with basicity of 2.5, S2—with basicity of 3.0, S3—with basicity of 3.5, S4—with basicity of 4.0, S5—with basicity of 4.5.

Moreover, by comparing and analyzing the mineral structure of S1–S5 slag samples, it was found that the number of CaS grains that precipitated along the silicate grain boundary in the S1 and S2 slag samples gradually decreased, while the CaS grains that precipitated in the matrix phase of S3–S5 slag samples were higher than S1 and S2 slag samples. The grain size of CaS increased gradually in the slag with the increase in basicity. The matrix phase in the solid slag was mainly distributed along the precipitated phase, and the distribution of the matrix phase in molten slag was mainly controlled by the precipitated phase. In addition, the number of CaS grains in the slag was statistically analyzed by image-ProPlus6.0, and the results are shown in Figure 7. When the slag basicity was 2.5, the number of CaS grains in the slag was 246, and when the slag basicity was 4.5, the number of CaS grains in the slag was 99. Thus, it can be seen that the number of CaS grains in molten slag gradually increased with the increase in basicity.

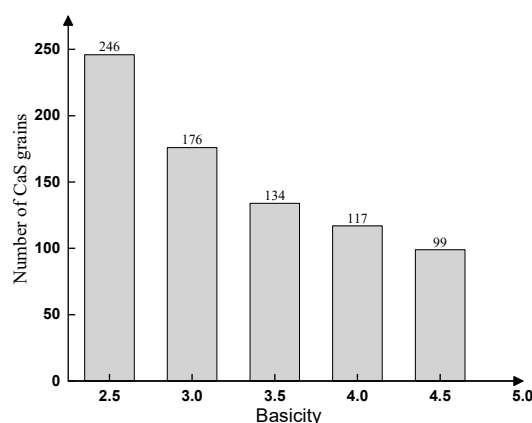


Figure 7. Number of CaS grains in molten slag.

5. Discussion

5.1. Effect of Basicity on the Sulfur Precipitation Behavior

When the basicity of the slag was 2.5–3.0, the slag contained separate C2S and C3S phases. This is mainly because the silicate formed by the slag reaction was in the C2S and C3S zones of CaO-SiO₂ phase diagram. When the slag basicity was equal to 3.5, 4.0 or 4.5, the silicate phase in the slag comprised a large area of massive the C3S phase. This was mainly because the silicate product in the slag was completely located in the C3S area in the CaO-SiO₂ phase diagram; the silicate product in the slag was mainly the C3S phase at 1600 °C. Moreover, the CaS grain size increased gradually with the increase in basicity due to the complex silicate network structure of slag decreased with the increase in basicity, which decreased the viscosity of slag, and promoted the growth of CaS grain in the slag. Certain scholars [22,23] have reported that an increase of CaO content in the slag led to the decrease of bridge oxygen content, which makes silicate network structure become simpler and decreases the viscosity of slag. Herein, the number of CaS grains in the slag samples decreased gradually with the increase in basicity due to the initial crystallization temperature of CaS decreased with the increase in basicity in the molten slag (Figure 4), which led to a decrease of the supercooling zone of CaS crystallization in the molten slag, leading to an increase of critical nucleation of CaS, and resulting in a gradual decrease in the nucleation rate of CaS crystals.

In addition, the precipitation behavior of the sulfur in the molten slags with different basicities was related to the nucleation mode of sulfur during solidification. The precipitation process of the sulfur in the molten slag included homogeneous and heterogeneous nucleation. Based on the above analysis of the microstructure of slags with different basicities, the sulfur in the solid slag was mainly distributed in the form of CaS in the matrix phase and grew along the grain boundary of the silicate. The CaS grains in the slags with low basicities ($R = 2.5$ and 3.0) mainly grew along the silicate grain boundary due to a large number of silicate solid particles existed in the matrix phase, which provided favorable conditions for the heterogeneous nucleation of sulfur in the matrix phase during precipitation. Jiang et al. [24] concluded that the existence of solid-phase ZrO₂ particles in CaO-Al₂O₃ slag causes heterogeneous nucleation of slag during solidification. Furthermore, the matrix phase of high-basicity slags ($R = 3.5$, 4.0 and 4.5) contained an amount of CaS grains, and several CaS grains grew along the silicate grain boundaries. This was mainly because the area of single silicate grains in the high-basicity slags was larger than that in the low-basicity slags, which reduced the contact area between the matrix phase and silicate solid particles, resulting in the precipitation process of CaS in high-basicity slags being mainly homogeneous nucleation. This implied that the precipitation of sulfur in the matrix phase of the low-basicity slags was mainly heterogeneous nucleation, while the CaS in high-basicity slags was mainly homogeneous nucleation.

5.2. Effect of Basicity on the Occurrence State of Sulfur in Slag

The micro-area distribution of the sulfur in the S1 and S3 slag samples in Figure 8 were analyzed by scanning electron microscopy (SEM-EDS), as shown. Through the surface scanning analysis data, it was found that the matrix phase around the CaS grains contained dispersed sulfur elements; thus, it can be determined that the slag matrix phase in the solidification process contained unprecipitated amorphous sulfur. The sulfur of the synthetic slag existed in two different states, namely, CaS crystal and amorphous sulfur. The sulfur elements distributed in the aggregated state of the molten slag were CaS crystals, while the sulfur elements distributed in the dispersed state occurred in the matrix phase as an amorphous structure. Comparing the microzone distribution of the sulfur elements in Figure 8a,b, it can be discovered that the amorphous structure density of the sulfur elements in the S3 slag sample was higher than that in the S1 slag sample, and the content of amorphous sulfur in the slag increased with an increase in basicity. The key reason of such a phenomenon was that the crystallization temperature of the CaS in the molten slag decreased with the increase in basicity and the supercooling zone of the CaS crystallization decreased during solidification in the same cooling system (air cooling), which reduced the amount of precipitation of the CaS phase and increased the amorphous sulfur content in matrix phase. Moreover, the thermodynamic calculation of sulfur precipitation during solidification in Figure 2 indicated that the sulfur in the slag was completely precipitated in the form of CaS, but the surface scanning distribution analytical results showed that the amorphous sulfur content of matrix phase increased with the increase in basicity. This was mainly because the kinetic condition of S^{2-} diffusion in the matrix phase deteriorated with the decrease in slag temperature during solidification, while certain S^{2-} in the matrix phase failed to diffuse to the surface of the CaS crystal nucleus to form CaS crystals and occurred in the form of an amorphous structure in matrix phase.

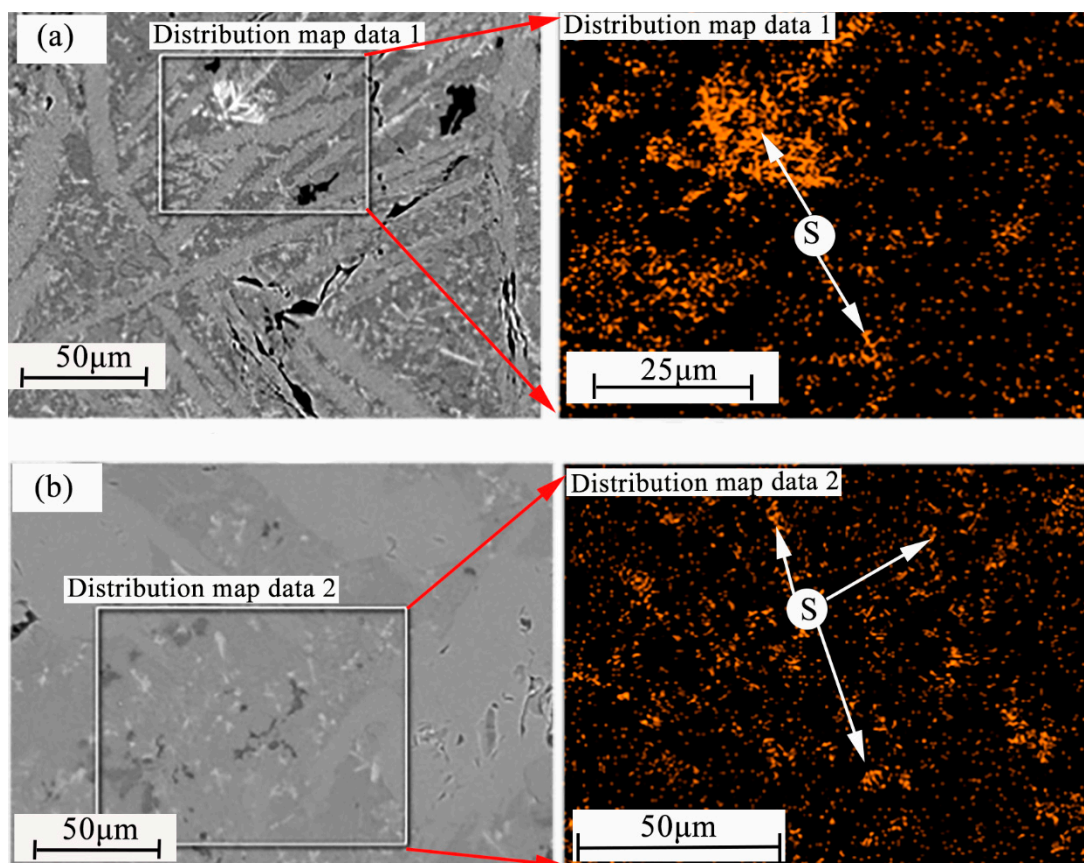


Figure 8. Surface scanning analysis of the sulfur elements in molten slag. (a) S1 with a basicity of 2.5, (b) S3 with a basicity of 3.5.

Based on the above, research status of KR desulfurization slag and the experimental results are discussed. At present, the comprehensive utilization process of KR desulfurization slag in China is not considered to remove sulfur from KR desulfurization slag and to reuse it in converter smelting processes. Therefore, the results are beneficial to provide a theoretical basis for the subsequent removal of sulfur from slag through oxidizing atmosphere.

6. Conclusions

- (1) According to the calculated results of molten slag solidification process based on thermodynamic database FactSage8.1, it was concluded that sulfur in KR desulfurization slag was mainly precipitated in the form of CaS, and the crystallization temperature of CaS in slag decreased with the increase of basicity;
- (2) CaS grains mainly precipitated along silicate grain boundaries in low-basicity ($R = 2.5$ and 3.0) slags, and the precipitation behavior of CaS was mainly heterogeneous nucleation. There were fewer CaS grains precipitated along silicate grain boundaries in molten slags with high basicity ($R = 3.5, 4.0$ and 4.5), and the precipitation behavior of sulfur in matrix phase was mainly homogeneous nucleation;
- (3) The number and the size of CaS grains decreased and increased respectively with the increase of the slag basicity.

Author Contributions: R.Z. drafted the manuscript and conducted the experiments, J.J. helped to conduct the experimental work, and J.L. modified and polished the draft. Y.Y. and H.Z. helped to read the manuscript. All authors have read and agreed to the published version of the manuscript.

Funding: The work was supported by the National Natural Science Foundation of China (No. 51974210, 52074197), the Hubei Provincial Natural Science Foundation (No. 2019CFB697), and the State Key Laboratory of Refractories and Metallurgy.

Acknowledgments: The authors would like to thank the National Natural Science Foundation of China and the Hubei Provincial Natural Science Foundation for their financial supports.

Conflicts of Interest: The authors declare no conflict of interest.

References

1. He, M.; Wang, N.; Chen, M.; Chen, M.; Li, C.F. Distribution and motion behavior of desulfurizer particles in hot metal with mechanical stirring. *J. Powder Technol.* **2019**, *361*, 455–461. [\[CrossRef\]](#)
2. Zhao, D.G.; Li, J.S.; Wang, S.H.; Liu, H.W.; Tong, Z.X.; Wu, F.P. Practical research on desulfurization in converter with the analysis of sulfur in steel for civil engineering. *J. Adv. Mater. Res.* **2012**, *56*, 17–20. [\[CrossRef\]](#)
3. Lv, B.; Zhang, F.C.; Li, M.; Hou, R.J.; Qian, L.H.; Wang, T.S. Effects of phosphorus and sulfur on the thermoplasticity of high manganese austenitic steel. *J. Mater. Sci. Eng. A* **2010**, *527*, 5648–5653. [\[CrossRef\]](#)
4. Iwamasa, P.K.; Fruehan, R.J. Effect of FeO in the slag and silicon in the metal on the desulfurization of hot metal. *J. Metall. Mater. Trans. B* **1997**, *28*, 47–57. [\[CrossRef\]](#)
5. Wang, J.; Ge, W.S.; Chen, L.; Huang, S.Q.; Fan, J.R.; Zhong, Z.H. Study on technology of KR desulfurization for hot metal with vanadium and titanium. *J. Adv. Mater. Res.* **2012**, *581*, 1077–1082. [\[CrossRef\]](#)
6. Nakai, Y.; Sumi, I.; Uno, H.; Kikuchi, N.; Kishimoto, Y. Effect of flux dispersion behavior on desulfurization of hot metal. *J. ISIJ Int.* **2010**, *50*, 403–410. [\[CrossRef\]](#)
7. Marissa, V.R.; Antonio, R.S.; Rodolfo, M.; Miguel, A.H.; Federico, C.A.; Javier, C.A. Hot metal pretreatment by powder injection of lime-based reagents. *J. Steel Res. Int.* **2001**, *72*, 173–182.
8. Barron, M.A.; Hilerio, I.; Medina, D.Y. Modeling and simulation of hot metal desulfurization by powder injection. *Open J. Appl. Sci.* **2015**, *5*, 295–303. [\[CrossRef\]](#)
9. Zhang, M.L.; Xu, A.J. Comparison of application of KR method with that of injection method in hot metal desulfurization. *J. Steelmaking* **2009**, *25*, 73–77. (In Chinese)
10. Tong, Z.B.; Ma, G.J.; Cai, X.; Xue, Z.L.; Wang, W. Characterization and valorization of kanbara reactor desulfurization waste slag of hot metal pretreatment. *Waste Biomass. Valoriz.* **2016**, *7*, 1–8. [\[CrossRef\]](#)
11. Han, Y.X.; Wang, L.Y.; Li, L.X.; Ren, F.; Zhao, C.Y.; Liu, X. Comprehensive utilization of slag from desulfurization and slag skimming processes of AnSteel. *J. Min. Metall. Eng.* **2009**, *29*, 29–32. (In Chinese)
12. Sheng, G.H.; Huang, P.; Wang, S.S.; Chen, G.G. Potential reuse of slag from the kanbara reactor desulfurization process of iron in an acidic mine drainage treatment. *J. Environ. Eng.* **2014**, *140*, 232–236. [\[CrossRef\]](#)

13. Maekelae, M.; Watkins, G.; Poeykioe, R.; Nurmesniemi, H.; Dahl, O. Utilization of steel, pulp and paper industry solid residues in forest soil amendment: Relevant physicochemical properties and heavy metal availability. *J. Hazard. Mater.* **2012**, *207*, 21–27. [[CrossRef](#)]
14. Kazuya, F.; Koichiro, O.; Taichi, M.; Eiki, K. Effective utilization of KR slag in iron ore sintering process. *J. Iron Steel Inst. Jpn.* **2017**, *103*, 357–364.
15. Nakai, Y.; Kikuchi, N.; Iwasa, M.; Nabeshima, S.; Kishimoto, Y. Development of slag recycling process in hot metal desulfurization with mechanical stirring. *J. Steel Res. Int.* **2009**, *80*, 727–732.
16. Wu, Q.F.; Bao, Y.P.; Lin, L.; XU, G.P.; Cheng, H.G.; Xin, C.P. Ineralogy characteristics and sulfur behavior of KR desulfurization slag. *J. China Metall.* **2015**, *25*, 44–47. (In Chinese)
17. Xue, H.M.; Li, J.; Xia, Y.J.; Wang, Y. Mechanism of phosphorus enrichment in dephosphorization slag produced using the technology of integrating dephosphorization and decarburization. *J. Met.* **2021**, *11*, 216–230.
18. Pahlevani, F.; Kitamura, S.Y.; Shibata, H.; Shibata, H.; Maruoka, N. Distribution of P₂O₅ between solid solution of 2CaO·SiO₂·3CaO·P₂O₅ and liquid phase. *J. ISIJ Int.* **2010**, *50*, 822–829. [[CrossRef](#)]
19. Kitamura, S.Y.; Saito, S.; Utagawa, K.; Shibata, H.; Robertson, D.G.C. Mass transfer of P₂O₅ between liquid slag and solid solution of 2CaO·SiO₂ and 3CaO·P₂O₅. *J. Trans. Iron Steel Inst. Jpn.* **2009**, *49*, 1838–1844. [[CrossRef](#)]
20. Jiang, T.F.; Zhu, L.; Liu, F.G.; Zhao, X.D.; Luo, Y.Z. Recycling of desulfurization slag in pretreatment of hot metal. *J. Iron Steel* **2017**, *52*, 24–27. (In Chinese)
21. Xu, J.F.; Wang, X.H.; Huang, F.X.; Liu, C.Y. Analysis of phase and distribution of sulfur in KR desulfurization slag. *J. Iron Steel* **2015**, *50*, 15–18. (In Chinese)
22. Zhou, L.J.; Wang, W.L.; Ma, F.J.; Jin, L.; Wei, J.; Hiroyuki, M.; Fumitaka, T. A Kinetic study of the effect of basicity on the mold fluxes crystallization. *J. Metall. Mater. Trans. B* **2012**, *43*, 354–362. [[CrossRef](#)]
23. Dong, J.M.; Tsukihashi, F. Recent advances in understanding physical properties of metallurgical slags. *J. Met. Mater. Int.* **2017**, *23*, 1–19.
24. Jiang, B.B.; Wang, W.L.; Sohn, I.; Wei, J. A kinetic study of the effect of ZrO₂ and CaO/Al₂O₃ ratios on the crystallization behavior of a CaO-Al₂O₃-based slag system. *J. Metall. Mater. Trans. B* **2014**, *45*, 1057–1067. [[CrossRef](#)]